JOURNAL OF GUIDANCE, CONTROL, AND DYNAMICS
Vol. 32, No. 6, November–December 2009

Engineering Notes

Vision-Based Obstacle Avoidance of Wheeled Robots Using Fast Estimation

Amanda Dippold*
Virginia Polytechnic Institute and State University, Blacksburg, Virginia 24060
Lili Ma†
Wentworth Institute of Technology, Boston, Massachusetts 02135
and
Naira Hovakimyan‡
University of Illinois at Urbana-Champaign, Urbana, Illinois 61801

DOI: 10.2514/1.46016

I. Introduction

THE application of mobile vehicles for military and commercial purposes has increased dramatically in recent years. To minimize human interaction, these vehicles must be able to execute robust and efficient obstacle detection and avoidance using onboard measurements. Inertial measurement units augmented with GPS have traditionally been used for onboard sensing in a wide variety of missions. The reliance of GPS on low-power radio signals from Earth-orbiting satellites makes it vulnerable to intentional (e.g., jamming) or unintentional (e.g., electrical) interference that can degrade system performance [1]. Alternatively, vision-based sensors are being used as they are low cost, light weight, and passive. Vision-based sensors require a robust estimation scheme. The extended Kalman filter (EKF) has been used widely for this purpose [2–7]. Application of the EKF requires linearization about the desired trajectory and is very sensitive to initial errors [8–10]. Improvements of EKF performance with application to obstacle avoidance have been reported in [8,9,11] by using unscented Kalman filters and sigma-point Kalman filters. However, convergence guarantees for the parameter and range estimation cannot be deduced from application of the EKF or its variations.

In this paper, we augment a baseline path-following controller with an online obstacle-avoidance algorithm such that the robot tracks a prespecified path and avoids isolated obstacles using only visual information collected from an onboard camera. The nonholonomic vehicle is a unicycle type that has two identical parallel, nondeformable rear wheels and a steering front wheel. A path-following controller is implemented that allows for global convergence results [12–14]. The obstacle-avoidance algorithm uses a potential function that yields larger values for paths that are close to obstacles and lower values for paths that are far from obstacles. In this sense, obstacles represent local maximums for the potential function and act as a "repellent force" on the prespecified path. The obstacle-avoidance scheme deforms the desired path away from obstacles, thereby decreasing the potential function [15–18].

Conventionally, algorithms for obstacle avoidance have been divided into path-planning algorithms and control algorithms. Path-planning approaches compute a continuous path based on a world model. They are generally computationally expensive, and their ability to handle changing or unknown environments is limited [19]. In contrast, sensor-based control approaches, which detect and avoid unknown obstacles during the execution of the motion, are able to react to sudden changes in the environment. The drawback to these methods is that they may be suboptimal because only local information is used [20]. A complete solution exploits the benefits of both methods by formulating the problem as a local path-planning problem. Local detours around sensed obstacles are generated while the vehicle follows the perturbed planned path. Artificial potential fields are widely used for generating these local detours. Potential field methods (PFM) are an attractive approach due to the methods' simplicity and efficiency in implementation [21]. PFM is introduced in [19] for holonomic vehicles and extended in [15–18] for nonholonomic vehicles.

The visual information collected by the camera is processed by an estimator that provides the inputs to the obstacle-avoidance algorithm. These inputs include estimation of the obstacle's position and size. These in turn command the direction of deformation and duration required for obstacle avoidance. An estimation of the obstacle's unknown position and size is obtained via a fast estimator with quantifiable performance bounds [22,23]. The effect of the estimator's performance on the obstacle-avoidance scheme is presented.

II. Path Following and Obstacle Avoidance

Consider a nonholonomic system of dimension n with kinematics of the form

$$\dot{x}(t) = X_0(x(t)) + X_1(x(t))u_1(t) + X_2(x(t))u_2(t) + \cdots + X_m(x(t))u_m(t) \tag{1}$$

where $x(t) \in \mathbb{R}^n$ is the state vector of the system, and $u_1(t)$, $u_2(t), \ldots, u_m(t)$ are the kinematic control inputs of the system for $m < n$. The vectors $X_1(x(t)), X_2(x(t)), \ldots, X_m(x(t))$ are the *control vector fields*, and the kinematic control inputs $(u_1(t), u_2(t), \ldots, u_m(t))$ are the elements of $\dot{x}(t)$ in the basis $(X_1(x(t)), \ldots, X_m(x(t)))$ [24]. The vector $X_0(x(t))$ is denoted as the *drift* of the system and for kinematic systems is equal to zero. For physical systems, such as the mobile robot example in this paper, $x(t)$ can represent a vector of the position and orientation of the vehicle, and $u_1(t), u_2(t), \ldots, u_m(t)$ can represent the vehicle's speed and rate of rotation.

For the purpose of path following, recall that a path is a curve $p\colon s \to \mathbb{R}^n$, where s is the abscissa along the path. An *admissible path* is a smooth curve in $\mathbb{R}^n$ defined over an interval $[0, S]$ such that there exist m-dimensional smooth mappings $u_1(s), u_2(s), \ldots, u_m(s)$ defined over $[0, S]$, with [24]

$$\frac{\mathrm{d}}{\mathrm{d}s}(p(s)) = \sum_{j=1}^{m} u_j(s)X_j(p(s)), \quad \forall\ s \in [0, S] \tag{2}$$

In this setup, the kinematic inputs $u_1(s), \ldots, u_m(s)$ are the coordinates of $\frac{\mathrm{d}}{\mathrm{d}s}(p(s))$, which can be viewed as the velocity vector at abscissa s along the current path $p(s)$ in the basis $(X_1(p(s)),$

Presented as Paper 7449 at the AIAA Guidance, Navigation and Control Conference and Exhibit, Honolulu, HI, 18–21 August 2008; received 16 June 2009; revision received 31 July 2009; accepted for publication 6 August 2009.

*Graduate Student, Department of Aerospace and Ocean Engineering. Student Member AIAA.
†Assistant Professor, Department of Electronics and Mechanical. Member AIAA.
‡Professor, Mechanical Science and Engineering. Member AIAA.

$\ldots, X_m(p(s)))$. The simplified vehicle kinematic equations of a mobile robot are

$$\begin{cases} \dot{x}_I(t) = v(t)\cos\psi(t) \\ \dot{y}_I(t) = v(t)\sin\psi(t) \\ \dot{\psi}(t) = r(t) \end{cases} \tag{3}$$

where $v(t)$ is the speed of the vehicle, $\psi(t)$ is the yaw angle, and $r(t)$ is the vehicle's rate of rotation. The coordinates $x_I(t)$ and $y_I(t)$ are expressed in a fixed inertial frame. A path following controller for the kinematics in Eq. (3) with global convergence properties has been presented in [12–14].

In the absence of obstacles, the vehicle follows the desired path, denoted by $p(s)$. To account for obstacles, a collision criterion must be introduced. The information required by the collision criterion is the range to obstacles and the size of the obstacles. When the collision criterion is violated, the vehicle veers from its original path $p(s)$ and follows a new path until it is deemed safe to revert back to its original path. It is assumed that the vehicle can only detect obstacles within a distance R_s to itself. For readability, the subscript s of R_s denotes sensor range. At any time t, the vehicle's visual sensors detect $l(t) \in \{0, 1, 2, \ldots\}$ obstacles. It is further assumed that each obstacle has circular shape with unknown radius $L_i \leq L_{\max}$, where $L_{\max}$ is a conservative upper bound. An additional "danger radius" R_{d_i} surrounds each obstacle and must be avoided to ensure the safety of the vehicle. That is, $R_{d_i} = L_i + d$, where d is an a priori specification.

Let (P_{x_i}, P_{y_i}) be the location of the ith obstacle in the inertial frame. Define the points

$$\begin{aligned} P_{1i}(t) &= -[P_{x_i} - x_I(t)]\sin\psi(t) + [P_{y_i} - y_I(t)]\cos\psi(t) + R_{d_i}(t) \\ P_{2i}(t) &= -[P_{x_i} - x_I(t)]\sin\psi(t) + [P_{y_i} - y_I(t)]\cos\psi(t) - R_{d_i}(t) \end{aligned} \tag{4}$$

and let $z_i(t)$ denote the measured distance from the vehicle to the ith obstacle. The points $P_{1i}(t)$ and $P_{2i}(t)$ lie on a line that intersects the location of the ith obstacle (P_{x_i}, P_{y_i}) and is perpendicular to the vehicle's velocity vector [25]. Hence, $P_{1i}(t)$ and $P_{2i}(t)$ are the extremities of the projected edge of the ith obstacle in the vehicle's body-fixed frame. The collision criterion is given as

$$\begin{aligned} &\text{If } z_i(t) \leq R_s \text{ and } \operatorname{sign}(P_{1i}(t)) \neq \operatorname{sign}(P_{2i}(t)) \\ &\quad \forall\ i \in \{1, 2, \ldots, l(t)\} \rightarrow \text{collision criterion violated} \end{aligned} \tag{5}$$

The insight behind this collision criterion is that, if a line extending from the vehicle's velocity vector intersects with any obstacle boundary, the vehicle will collide with the obstacle and the path must be modified.

To compute a new path, we adopt a reactive obstacle-avoidance method in [15–18] that deforms the original path on a kinematic level in real time to move away from obstacles and ensures that the new path is collision free. The main idea of this path deformation algorithm is to iteratively deform a path $p(s)$ by perturbing the kinematic inputs $u_j(s)$ introduced in Eq. (2). In that respect, a positively increasing parameter $\tau \in [0, +\infty)$ is introduced to index these iterations. The original path $p(s)$ then corresponds to the case when $\tau = 0$ and is rewritten as $p(s) = p(s, 0)$. The path-deformation process is modeled as a mapping from a subset of $[0, S] \times [0, +\infty)$ to $\mathbb{R}^n$ composed entirely of admissible paths. That is, there exist m-dimensional smooth mappings $u_1(s, \tau), u_2(s, \tau), \ldots, u_m(s, \tau)$ defined over $[0, S] \times [0, +\infty)$ such that

$$\begin{aligned} \frac{\partial}{\partial s}(p(s,\tau)) &= \sum_{j=1}^{m} u_j(s,\tau) X_j(p(s,\tau)) \\ &\forall\ (s,\tau) \in [0,S] \times [0,+\infty) \end{aligned} \tag{6}$$

Differentiating Eq. (6) with respect to τ, we get

$$\begin{aligned} \frac{\partial^2}{\partial s \partial \tau}(p(s,\tau)) = \sum_{j=1}^{m} \Bigg(&\frac{\partial u_j}{\partial \tau}(s,\tau) X_j(p(s,\tau)) \\ &+ u_j(s,\tau) \frac{\partial X_j}{\partial p}(p(s,\tau)) \frac{\partial p}{\partial \tau}(s,\tau) \Bigg) \end{aligned} \tag{7}$$

Let $\nu(s, \tau)$: $[0, S] \times [0, +\infty) \mapsto \mathbb{R}^m$ and $\kappa(s, \tau)$: $[0, S] \times [0, +\infty) \mapsto \mathbb{R}^n$ denote the *input perturbations* and the *direction of deformation*, respectively,

$$\nu(s,\tau) \triangleq \frac{\partial u}{\partial \tau}(s,\tau), \qquad \kappa(s,\tau) \triangleq \frac{\partial p}{\partial \tau}(s,\tau) \tag{8}$$

where $u \triangleq [u_1, u_2, \ldots, u_k]^\top$. The direction of deformation is shown in Fig. 1.

Restrict $\nu(s, \tau)$ to a finite dimensional subspace of C^∞ generated by q linearly independent basis functions $\{b_1(s), b_2(s), \ldots, b_q(s)\}$ as

$$\nu(s,\tau) = \sum_{j=1}^{q} \lambda_j(\tau) b_j(s) \tag{9}$$

where the choice of appropriate parameters $\lambda_j(\tau)$ depends upon a local potential field $U(p(s, \tau))$ and a global potential function that sums up this potential field along the path

$$Y(\tau) = \int_0^S U(p(s,\tau))\, \mathrm{d}s \tag{10}$$

Given a potential field $U(p(s, \tau))$, an initial path $p(s, 0)$, and the obstacle location, the path-deformation algorithm iterates with respect to τ until the potential function no longer decreases from further iterations and all collisions with obstacles have been avoided. The output is a new path $p(s, \tau)$.

To define the obstacle-avoidance path, a portion of the original path $p(s)$ is deformed in the direction that minimizes a given potential function chosen to achieve the specific goal of obstacle avoidance. One such choice of the potential function in Eq. (10) can be

$$\begin{aligned} U(s,\tau) &= \sum_{i=1}^{l(s)} \mu_i(s,\tau) \\ \mu_i(s,\tau) &= \begin{cases} \frac{1}{\bar{z}_i(s,\tau)+d_0} + \frac{\bar{z}_i(s,\tau)}{(d_0+\hat{R}_d(t_1))^2}, & \text{if } 0 \leq \bar{z}_i(s,\tau) \leq \hat{R}_d(t_1), \\ \frac{1}{\hat{R}_d(t_1)+d_0} + \frac{\hat{R}_d(t_1)}{(d_0+\hat{R}_d(t_1))^2}, & \text{otherwise} \end{cases} \end{aligned} \tag{11}$$

where t_1 is a time the collision criterion in Eq. (5) is violated, $d_0 \ll 1$ is a constant, and

$$\bar{z}_i(s,\tau) = \sqrt{[p_x(s,\tau) - P_{x_i}(t_1)]^2 + [p_y(s,\tau) - P_{y_i}(t_1)]^2} \tag{12}$$

The parameter $\hat{R}_{d_i}(t)$, to be presented in Sec. III, is used by the vehicle as the estimate of R_{d_i} and is related to the estimation of L_i.

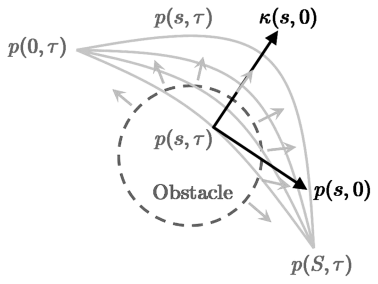

Fig. 1 The iterative path-deformation procedure. Obstacles impose repellent forces on the path so that the direction of deformation of the path ensures that an obstacle-avoidance potential function diminishes.

Choosing the potential function this way yields higher values when the vehicle is close to an obstacle and lower values when far away.

Remark 1: The definition of the potential field in Eq. (11) implies that the path will deform until $\bar{z}_i(s,\tau) > \hat{R}_d(t_1)$ for all $s \geq 0$. Indeed, $\bar{z}_i(s,\tau) > \hat{R}_d(t_1)$ everywhere implies that $U(s,\tau) = U$ is a constant for which the partial derivative with respect to the path equals zero. Hence, the direction of deformation $\kappa(s,\tau) = 0$ so that no further updates will be made.

Remark 2: The original undeformed path may be computed based on certain optimality criterion, and diverting away from this path decreases the optimality of the path. It can be seen from Eq. (11) that smaller values of $\hat{R}_{d_i}(t)$ restrict the path's deformation less far away from the original path, whereas larger values increase the distance between the vehicle and obstacles. Thus, there exists a tradeoff between increasing the safety margin for the vehicle and retaining the desired characteristics of the original path.

III. Vision-Based Range Identification

The vision-based range identification problem is formulated in a two-dimensional setting. Consider the two-dimensional scenario of a vision-based range identification problem as shown in Fig. 2. It is assumed that a conventional pinhole model for the camera is used and the camera is calibrated beforehand. Further, the obstacle is within the vehicle's sensor range and some image processing algorithms are available to extract the bearing angle $\beta(t)$ and the subtended angle $\alpha(t)$. The objective is to estimate the relative range $z(t)$ between the vehicle and the obstacle using the visual measurements $\alpha(t)$ and $\beta(t)$, as well as $\psi(t)$, $r(t)$, and $v(t)$, which are available from the vehicle's onboard sensors. To estimate the relative range between the vehicle and an obstacle, a fast-estimation scheme is used [22,23]. The effect of the estimated parameters on the obstacle avoidance is also discussed. This note also analyzes the system performance in the presence of out-of-frame events, when continuous extraction of the target's information is not feasible due to failures in the image processing module. The out-of-frame events are modeled as brief instabilities [26–29].

A. Estimation for Obstacle Avoidance

Let $(z_x(t), z_y(t))$ be the vector of relative distance between the vehicle and the obstacle in the inertial frame so that $z(t) = \sqrt{z_x^2(t) + z_y^2(t)}$. The quantities $z_x(t)$, $z_y(t)$, $\alpha(t)$, $\beta(t)$, and $z(t)$ are defined with respect to the inertial frame. In the kinematic setting, the relative dynamics are given by

$$\begin{cases} \dot{z}_x(t) = \dot{P}_x - \dot{x}_I(t) = -v(t)\cos\psi(t) \\ \dot{z}_y(t) = \dot{P}_y - \dot{y}_I(t) = -v(t)\sin\psi(t) \\ \dot{\psi}(t) = r(t) \end{cases} \tag{13}$$

The bearing angle $\beta(t)$ and the subtended angle $\alpha(t)$ are

$$\beta(t) = \psi(t) - \tan^{-1}\left(\frac{z_y(t)}{z_x(t)}\right), \qquad \alpha(t) = 2\tan^{-1}\left(\frac{L}{z(t)}\right) \tag{14}$$

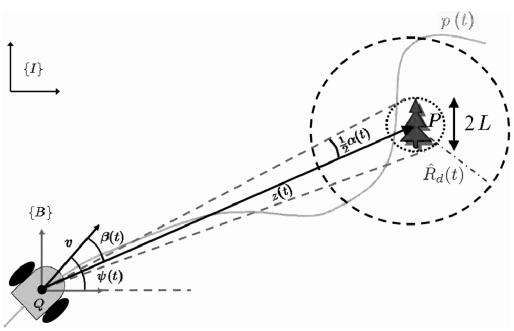

Fig. 2 Vision-based range identification.

Note from the definition of $\alpha(t)$ that $0 < \alpha(t) < \pi$ for all $t \geq 0$. If L is known, $z(t)$ can be computed from

$$z(t) = \frac{L}{\tan(\alpha(t)/2)} \tag{15}$$

Thus, knowledge of $z(t)$ is equivalent to knowledge of L because $\alpha(t)$ is measurable. It follows from Eqs. (13) and (14) and the definition of $z(t)$ that

$$\begin{aligned} \dot{z}_x(t) &= \frac{\partial z_x}{\partial \alpha}(t)\dot{\alpha}(t) + \frac{\partial z_x}{\partial \beta}(t)\dot{\beta}(t) + \frac{\partial z_x}{\partial \psi}(t)\dot{\psi}(t) = -v(t)\cos\psi(t) \\ \dot{z}_y(t) &= \frac{\partial z_y}{\partial \alpha}(t)\dot{\alpha}(t) + \frac{\partial z_y}{\partial \beta}(t)\dot{\beta}(t) + \frac{\partial z_y}{\partial \psi}(t)\dot{\psi}(t) = -v(t)\sin\psi(t) \end{aligned} \tag{16}$$

Solving Eq. (16) for $\dot{\alpha}(t)$ and $\dot{\beta}(t)$, we can have [23]

$$\begin{bmatrix} \dot{\alpha}(t) \\ \dot{\beta}(t) \end{bmatrix} = \underbrace{\theta \begin{bmatrix} f_1(t) \\ f_2(t) \end{bmatrix}}_{\omega(t)} + \underbrace{\begin{bmatrix} 0 \\ r(t) \end{bmatrix}}_{\phi(t)} \tag{17}$$

where

$$\begin{aligned} f(t) = \begin{bmatrix} f_1(t) \\ f_2(t) \end{bmatrix} &= \begin{bmatrix} 2v(t)\sin^2(\frac{\alpha(t)}{2})\cos\beta(t) \\ v(t)\tan(\frac{\alpha(t)}{2})\sin\beta(t) \end{bmatrix} \\ \theta = \frac{1}{L}, \qquad \omega(t) &= \begin{bmatrix} \omega_1(t) \\ \omega_2(t) \end{bmatrix} \end{aligned} \tag{18}$$

The estimation objective is to estimate the unknown parameter θ, upon which Eq. (15) yields the value of $\hat{z}(t)$, which is the estimate of the relative range between the vehicle and an obstacle.

A fast-estimation scheme is applied for the range identification problem formulated in Sec. III. The fast estimator allows for fast adaptation of the unknown parameter via a large adaptation gain and low-pass filter [22,23]. Considering Eq. (17), the signal $\omega(t)$ is uniformly bounded and continuously differentiable with a uniformly bounded derivative. That is, there exist positive constants μ_ω and d_ω such that

$$\|\omega(t)\| \leq \mu_\omega < \infty \quad \text{and} \quad \|\dot{\omega}(t)\| \leq d_\omega < \infty, \quad \forall\ t \geq 0 \tag{19}$$

Let

$$\begin{aligned} x(t) = [\alpha(t), \beta(t)]^\top, \qquad \hat{x}(t) = [\hat{\alpha}(t), \hat{\beta}(t)]^\top \\ \tilde{x}(t) = \hat{x}(t) - x(t) \end{aligned} \tag{20}$$

An estimate of $\omega(t)$, denoted by $\omega_e(t) = [\omega_{e_1}(t), \omega_{e_2}(t)]^\top$, can be obtained via the following steps.

1) *State Predictor*:

$$\dot{\hat{x}}(t) = A_m\tilde{x}(t) + \phi(t) + \hat{\omega}(t), \qquad \hat{x}(0) = x_0 \tag{21}$$

where A_m is a known Hurwitz matrix and $\hat{\omega}(t)$ are governed by the following update law.

2) *Update Law*:

$$\dot{\hat{\omega}}(t) = \Gamma_c\,\mathrm{Proj}\,(\hat{\omega}(t), -P\tilde{x}(t)), \qquad \hat{\omega}(0) = \hat{\omega}_0 \tag{22}$$

where $\Gamma_c \in \mathbb{R}^+$ is the adaptation gain and P is the solution of $A_m^\top P + PA_m = -Q$, $Q > 0$.

3) *Application of Low-Pass Filter*: The estimate of the unknown signal is generated by

$$\omega_e(s) = C(s)\hat{\omega}(s), \qquad \omega_e(0) = \hat{\omega}_0 \tag{23}$$

where $C(s)$ is a diagonal matrix with its ith diagonal element $C_i(s)$ being a strictly proper stable transfer function with low-pass gain $C_i(0) = 1$. One simple choice is

$$C_i(s) = c/(s+c), \qquad c > 0 \tag{24}$$

Knowledge of $\omega_e(t)$ implies that one can solve for $\hat{\theta}(t)$, the estimate of θ, using the relationship

$$\hat{\theta}(t) = \sqrt{\frac{\omega_{e_1}(t)^2 + \omega_{e_2}(t)^2}{f_1^2(t) + f_2^2(t)}} \tag{25}$$

4) *Range Identification*: The range between the vehicle and an obstacle can be computed via

$$\hat{z}(t) = \frac{\hat{\theta}^{-1}(t)}{\tan(\alpha(t)/2)} \tag{26}$$

Given an estimate for $z(t)$ and the measurements for $\beta(t)$ and $\psi(t)$, Eqs. (4–12) are redefined by replacing the unknown position of the obstacle $(P_x(t), P_y(t))$ with its estimate $(\hat{P}_x(t), \hat{P}_y(t))$, given by

$$(\hat{P}_x(t), \hat{P}_y(t)) = (\hat{z}(t)\cos(\psi(t) - \beta(t)), \hat{z}(t)\sin(\psi(t) - \beta(t))) \tag{27}$$

The fast estimator ensures that $\omega_e(t)$ estimates the unknown signal $\omega(t)$ with the following precision [22,23]:

$$\|\omega_e(t) - \omega(t)\|_\infty \leq \underbrace{\|\hat{\omega}_0 - \omega_0\|_\infty e^{-ct} + \|1 - C(s)\|_{\mathcal{L}_1}\|\omega\|_{\mathcal{L}_\infty} + \frac{\gamma_c}{\sqrt{\Gamma_c}}}_{\gamma_1(t)}, \quad \forall\ t \geq 0 \tag{28}$$

where $\|\cdot\|_{\mathcal{L}_\infty}$ denotes the $\mathcal{L}_\infty$ norm of a signal, $\|\cdot\|_{\mathcal{L}_1}$ denotes the $\mathcal{L}_1$ norm of the system [30], and

$$\gamma_c = \|C(s)H^{-1}(s)\|_{\mathcal{L}_1}\sqrt{\frac{\omega_m}{\lambda_{\min}(P)}}$$
$$\omega_m = 4\mu_\omega^2 + 4\mu_\omega d_\omega \frac{\lambda_{\max}(P)}{\lambda_{\min}(Q)}$$
$$H(s) = (s\mathbb{I} - A_m)^{-1} \tag{29}$$

where $\mathbb{I}$ denotes an identity matrix of appropriate dimension. Further, it was shown in [31] (Proposition 11, pp. 103–104) that if the Hurwitz matrix A_m is a diagonal matrix of the form $A_m = \mathrm{diag}(a_{m1}, a_{m2})$, where a_{m1}, a_{m2} are negative constants, then γ_c in Eq. (29) is independent of c. Then, it follows from Eqs. (28) and (29) that the bandwidth of $C(s)$ and the adaptation gain Γ_c are independent of each other. Increasing the adaptation gain Γ_c renders the term $\gamma_c/\sqrt{\Gamma_c}$ arbitrarily small. Notice that increasing the adaptation gain Γ_c requires faster computation and a smaller integration step. Further, increasing the bandwidth of $C(s)$ renders the term $\|1 - C(s)\|_{\mathcal{L}_1}$ arbitrarily small.

Remark 1: Notice that, if $|v(t)| > 0$ for all $t \geq 0$, the values of $f_1(t)$ and $f_2(t)$ cannot both be equal to zero at any time instance. If $v(t) = 0$, the estimation of θ is irrelevant. Therefore, Eq. (25) is always well defined. Because the vehicle is following a desired trajectory with a desired speed profile, the speed of the vehicle cannot remain zero for all time and estimation will be achieved for any nonzero velocity.

Remark 2: By replacing the original quantities $(P_x(t), P_y(t))$ and $z(t)$ with their estimates and generating new portions of the path via the obstacle-avoidance algorithm, the stability and convergence properties of the path-following controller are not lost. The path-following errors will be discontinuous whenever the path changes, but the stability will hold independent of changes in the path as long as the path itself is not discontinuous, which is guaranteed by imposing the same boundary conditions.

Proper estimation of the danger radius $\hat{R}_d(t)$ is essential to ensure obstacle avoidance. The value of $\hat{R}_d(t)$ is related to the estimate of the obstacle's size L. For safety considerations, the estimate $\hat{R}_d(t)$ must assume larger values as compared with R_d. One could choose $\hat{R}_d(t) = L_{\max} + d$, where $L_{\max}$ is an upper bound on L and d is an a priori specified constant, which would guarantee that $\hat{R}_d(t) \geq R_d$ for all ≥ 0. However, this represents the worst-case scenario and assumes the largest possible value for the obstacle. The new path would lead the vehicle farther away from the obstacle than needed. To reduce this additional cost, $\hat{R}_d(t) \geq R_d$ can be derived using the fast estimator that takes into account the obstacle's estimated size, resulting in a less conservative estimate for R_d. It follows from Eq. (25) and the inequality in (28) that

$$\|\hat{\theta}(t) - \theta\|_\infty = \left\|\frac{1}{\hat{L}(t)} - \frac{1}{L}\right\|_\infty \leq \frac{\|\omega_e(t) - \omega(t)\|_\infty}{\sqrt{f_1^2(t) + f_2^2(t)}}$$
$$\leq \underbrace{\frac{\gamma_1(t)}{\sqrt{f_1^2(t) + f_2^2(t)}}}_{\gamma_2(t)} < \infty, \quad \forall\ t \geq 0 \tag{30}$$

Hence, $\|\hat{L}(t) - L\|_\infty \leq \hat{L}(t)L\gamma_2(t) \leq L_{\max}^2\gamma_2(t)$ for all $t \geq 0$. The following proposition holds.

Proposition 1: In the application of the fast estimator, if the estimate $\hat{R}_d(t)$ of R_d is chosen as

$$\hat{R}_d(t) = \hat{L}(t) + d + L_{\max}^2\gamma_2(t) \tag{31}$$

where $\gamma_2(t)$ is the bounded term defined in inequality (30), then $\hat{R}_d(t) \geq R_d$ for all $t \geq 0$.

Proof:

$$\hat{R}_d(t) - R_d = \hat{L}(t) + d + L_{\max}^2\gamma_2(t) - (L + d) = \hat{L}(t) - L + L_{\max}^2\gamma_2(t) \geq -\|\hat{L}(t) - L\|_\infty + L_{\max}^2\gamma_2(t) \geq 0 \tag{32}$$

□

Remark 3: It can be seen that, at $t = 0$, the estimate $\hat{R}_d(t)$ is more conservative than $\hat{R}_d(t) = L_{\max} + d$. However, the bandwidth of the low-pass filter $C(s)$ can be increased so that the first term in $\gamma_1(t)$ decreases exponentially as $t \to \infty$. The additional terms that appear in the application of the fast estimator can be made arbitrarily small by increasing c and the adaptation gain Γ_c so that the estimate $\hat{R}_d(t)$ is close to the estimated size of the obstacle $\hat{L}(t)$ and is less than $L_{\max} + d$.

B. Estimation in the Presence of Out-of-Frame Events

In vision-based applications, target information obtained from continuous extraction is often unavailable due to environmental factors, limited field of view of the camera, or failure in the image-processing module. These phenomena are commonly referred to as out-of-frame events. Following [26–29], define the tracking loss as a binary signal

$$s(t) := \begin{cases} 0 & \text{out-of-frame events at time } t, \\ 1 & \text{camera tracks the target at time } t \end{cases} \tag{33}$$

Let $T_s(\tau, t)$ denote the amount of time in the interval $[\tau, t]$ when $s(t) = 0$. Formally,

$$T_s(\tau, t) := \int_\tau^t (1 - s(t'))\,\mathrm{d}t'$$

We say that the image processing experiences brief target loss if $T_s(\tau, t) \leq T_0 + \alpha(t - \tau), \ \forall\ t \geq \tau \geq 0$, for some $T_0 \geq 0$ and $\alpha \in [0, 1]$. The scalar T_0 is called the instability bound and α is called the asymptotic instability ratio (p. 891 of [26]).

When the target is out of frame, we do not have the measurement for $\alpha(t)$ and $\beta(t)$. In this case, the path-deformation algorithm uses the latest available estimate $\hat{\omega}(t)$ for the unknown parameters, treating it as constant. That is, referring to Eq. (22), we let $\dot{\hat{\omega}}(t) = 0$ when $s(t) = 0$. The state estimator and the update law in the presence of target loss become the following.

1) *State Predictor*:

$$\dot{\hat{x}}(t) = s(t)A_m\tilde{x}(t) + \phi(t) + \hat{\omega}(t) \tag{34}$$

where $s(t)$ is defined in Eq. (33). Notice that, when the visual measurements become available at time instant t_i, the initial state of $\hat{x}(t_i)$ is then set as $\hat{x}(t_i) = x(t_i)$.

2) *Update Law*:

$$\dot{\hat{\omega}}(t) = \Gamma_c \,\mathrm{Proj}\,(\hat{\omega}(t), -s(t)P\tilde{x}(t)) \tag{35}$$

Equations (23–26) remain the same.

The performance of the fast estimator in the presence of out-of-frame events is analyzed. Consider two subsystems. One subsystem corresponds to the case in which the visual measurements are available, referred to as $\mathcal{G}_1$ hereafter, for $s(t) = 1$. The other subsystem corresponds to the case of the out-of-frame events for $s(t) = 0$. To quantify the performance bound of the fast estimator, an intermediate signal $\omega_r(t)$ is introduced as

$$\omega_r(s) = C(s)\omega(s), \qquad \omega_r(0) = \hat{\omega}_0 \tag{36}$$

It was shown in [22] that $\|\omega_r(t) - \omega(t)\|_\infty \le \|\hat{\omega}_0 - \omega_0\|_\infty e^{-ct} + \|1 - C(s)\|_{\mathcal{L}_1}\|\omega\|_{\mathcal{L}_\infty}$. Then,

$$\begin{aligned}\|\omega_e(t) - \omega(t)\|_\infty &\le \|\omega_e(t) - \omega_r(t)\|_\infty \\ &\quad + \|\omega_r(t) - \omega(t)\|_\infty \le \|\omega_e(t) - \omega_r(t)\|_\infty \\ &\quad + \|\hat{\omega}_0 - \omega_0\|_\infty e^{-ct} + \|1 - C(s)\|_{\mathcal{L}_1}\|\omega\|_{\mathcal{L}_\infty}\end{aligned} \tag{37}$$

It remains to derive the performance bound $\|\omega_e(t) - \omega_r(t)\|_\infty$.

Considering subsystem $\mathcal{G}_1$, it follows from Eqs. (23) and (36) that

$$\dot{\omega}_e(t) = -c\omega_e(t) + c\hat{\omega}(t), \qquad \dot{\omega}_r(t) = -c\omega_r(t) + c\omega(t) \tag{38}$$

Thus,

$$\dot{\omega}_e(t) - \dot{\omega}_r(t) = -c(\omega_e(t) - \omega_r(t)) + c(\hat{\omega}(t) - \omega(t)) \tag{39}$$

Further, it was shown in [22] that $\|\omega_e(t) - \omega_r(t)\|_\infty \le \gamma_c/\sqrt{\Gamma_c}$, where γ_c and Γ_c are given in Eq. (29). With the following candidate Lyapunov function

$$V(t) = \frac{[\omega_e(t) - \omega_r(t)]^\top[\omega_e(t) - \omega_r(t)]}{2} \tag{40}$$

one can have

$$\begin{aligned}\dot{V}(t) &= [\omega_e(t) - \omega_r(t)]^\top[\dot{\omega}_e(t) - \dot{\omega}_r(t)] \\ &= [\omega_e(t) - \omega_r(t)]^\top[-c(\omega_e(t) - \omega_r(t)) + c(\hat{\omega}(t) - \omega(t))] \\ &= -2cV(t) + c[\omega_e(t) - \omega_r(t)]^\top[\hat{\omega}(t) - \omega(t)] \\ &\le -\alpha_1 V(t) + \xi_1\end{aligned} \tag{41a}$$

with

$$\alpha_1 = 2c, \qquad \xi_1 = 2c\mu_\omega\gamma_c/\sqrt{\Gamma_c} \tag{41b}$$

where $\|\hat{\omega}(t) - \omega(t)\| \le 2\mu_\omega$ is ensured by the projection-type operator. Next, considering subsystem $\mathcal{G}_2$, it can be verified that there exists a positive constant M_d such that $\|\dot{\omega}_e(t) - \dot{\omega}_r(t)\| \le M_d$. Using the same Lyapunov function in Eq. (40), one can obtain

$$\dot{V}(t) = [\omega_e(t) - \omega_r(t)]^\top[\dot{\omega}_e(t) - \dot{\omega}_r(t)] \le V(t) + M_d^2/2 \tag{42}$$

Therefore,

$$\dot{V}(t) \le \alpha_2 V(t) + \xi_2 \tag{43a}$$

with

$$\alpha_2 = 1, \qquad \xi_2 = M_d^2/2 \tag{43b}$$

Combining inequalities (41) and (43) leads to

$$\dot{V}(t) \le \begin{cases} -\alpha_1 V(t) + \xi_1 = -(\alpha_1 - \frac{\xi_1}{V(t)})V(t), & \text{subsystem } \mathcal{G}_1 \\ \alpha_2 V(t) + \xi_2 = (\alpha_2 + \frac{\xi_2}{V(t)})V(t), & \text{subsystem } \mathcal{G}_2 \end{cases} \tag{44}$$

Let

$$V_b = \frac{\xi_1}{\alpha_1} + \epsilon_b$$

where $\epsilon_b > 0$ is a small positive constant. If $V(t) > V_b$,

$$\dot{V}(t) \le \begin{cases} -\lambda_0 V(t), \lambda_0 = \alpha_1 - \xi_1/V_b, & \text{subsystem } \mathcal{G}_1 \\ \mu V(t), \mu = \alpha_2 + \xi_2/V_b, & \text{subsystem } \mathcal{G}_2 \end{cases} \tag{45}$$

Similar to the derivations of Theorem 3 in [28], the following theorem establishes the stability of the switched system consisting of the two subsystems $\mathcal{G}_1$ and $\mathcal{G}_2$. Please see the Appendix for the derivations.

Theorem 1: Assume that the switched system consisting of Eqs. (41) and (43) has brief instability with an instability bound T_0 and an asymptotic instability ratio α that satisfy

$$\alpha < \alpha^* = \lambda_0/(\lambda_0 + \mu) \tag{46a}$$

$$T_0 < \log(V_\Omega/V_b)/(\lambda_0 + \mu) \tag{46b}$$

where

$$V_b = (\xi_1/\alpha_1) + \epsilon_b \tag{47}$$

subject to

$$0 < \epsilon_b < V_\Omega - \xi_1/\alpha_1 \tag{48}$$

with $V_\Omega = 4\mu_\omega^2$. Then, the switched system consisting of subsystems $\mathcal{G}_1$ and $\mathcal{G}_2$ is uniformly ultimately bounded with the ultimate bound given by $e^{(\lambda_0+\mu)T_0}V_b$ for every initial value inside the region of attraction given by $\Omega = \{\omega_e(0) - \omega_r(0)\colon \|\omega_e(0) - \omega_r(0)\| < 2\mu_\omega\}$.

It follows from Theorem 1 and inequality (37) that, in the presence of out-of-frame events, the fast estimator estimates the unknown signal $\omega(t)$ with the following precision:

$$\begin{aligned}\|\omega_e(t) - \omega(t)\|_\infty &\le \sqrt{e^{(\lambda_0+\mu)T_0}V_b} + \|\hat{\omega}_0 - \omega_0\|_\infty e^{-ct} \\ &\quad + \|1 - C(s)\|_{\mathcal{L}_1}\|\omega\|_{\mathcal{L}_\infty} \triangleq \gamma_1(t), \quad \forall\ t \ge 0\end{aligned} \tag{49}$$

Let

$$\bar{\gamma}_2(t) = \frac{\bar{\gamma}_1(t)}{\sqrt{f_1^2(t) + f_2^2(t)}} \tag{50}$$

The analysis through Eqs. (30–32) can be repeated for the case with the target loss by replacing $\gamma_1(t)$ and $\gamma_2(t)$ with $\bar{\gamma}_1(t)$ and $\bar{\gamma}_2(t)$, respectively.

IV. Simulation Results

Path following with vision-based obstacle avoidance is implemented in MATLAB®. The desired path is computed using two fifth-order polynomial curves. There are two isolated obstacles at $P_1 = (8, 1)$ and $P_2 = (20, 2.5)$ with $L_1 = 1$ and $L_2 = 2.5$. For path deformation, $d_0 = 0.001$. The sensor radius is chosen to be $R_s = 5$ and $d = 1$. Fast-estimator parameters are $L_{\min} = 0.5$, $L_{\max} = 2$, $\hat{\omega}(0) = [0.008, 0.008]^\top$, $A_m = -5 \times \mathbb{I}_2$, $Q = 2 \times \mathbb{I}_2$, $\Gamma_c = 7500$, and $c = 50$. All quantities conform to a given unit system, for instance, meter, meter per second, etc.

Simulation results are presented in Fig. 3, in which the visual measurements are corrupted by 1% uniform noise and the out-of-frame signal is of 10% of every 2 s interval. It can be seen from Fig. 3a that the path diverts from its original path, avoids the obstacle, and reverts back to the original path when the vehicle is outside the sensor

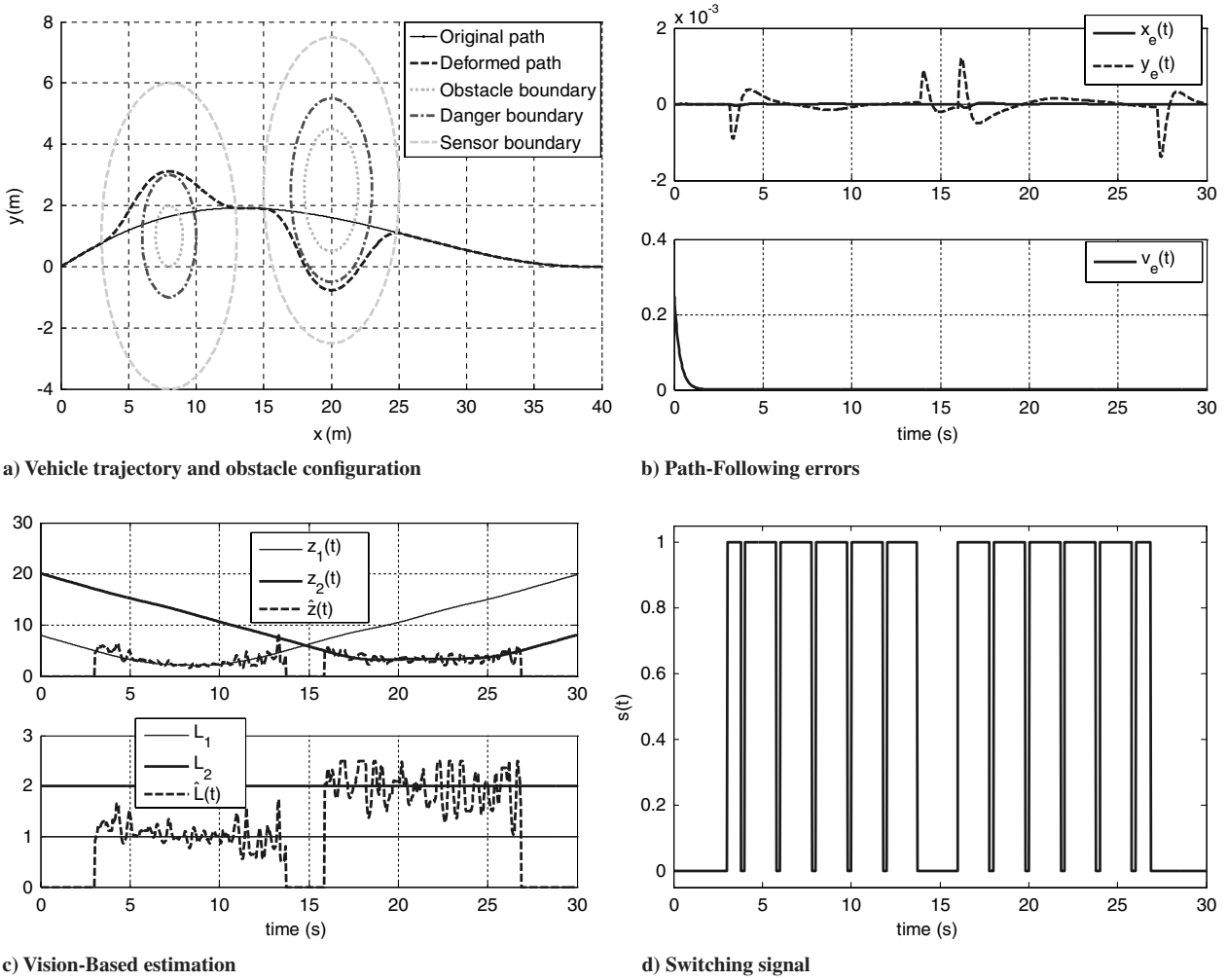

a) Vehicle trajectory and obstacle configuration

b) Path-Following errors

c) Vision-Based estimation

d) Switching signal

Fig. 3 Path following with vision-based obstacle avoidance in the presence of measurement noise and out-of-frame events.

range R_s. Figure 3b shows the path-following errors, where $x_e(t)$ and $y_e(t)$ denote the x and y coordinates of the path-following errors between the vehicle and a virtual vehicle, and $v_e(t)$ is the error between $v(t)$ and a desired velocity profile [23]. Discontinuities occur in four places: when the path changes to avoid each obstacle and when the path reverts back to the original path after each obstacle has been avoided. Figure 3c shows an estimation of the obstacles' unknown sizes via fast estimator, for which the obstacles' sizes are kept "frozen" during target loss. Figure 3d shows the corresponding out-of-frame signal $s(t)$.

V. Conclusions

This paper considers path deformation for static obstacle avoidance and vision-based estimation for a mobile robot equipped with a single camera. A fast-estimation scheme that achieves fast convergence speed with quantifiable bounds is applied to solve the range identification problem. The paper also analyzes the performance degradation of the fast estimator in the presence of out-of-frame events, modeled as brief instabilities. A sufficient condition for the switching signal is derived that guarantees graceful degradation of estimation performance during target loss.

Appendix: Proof of Theorem 1

First, notice that $\xi_1/\alpha_1 < V_\Omega$, so that the choice of ϵ_b in inequality (48) is valid. It follows from Eqs. (47) and (48) that $V_b < V_\Omega$; as a result, the right-hand side of inequality (46b) is greater than zero so that Eq. (46b) is valid. Second, it will be shown by contradiction that the trajectory of the switched system remains inside the region of attraction Ω. Then, the corresponding ultimate bound is quantified.

Because $V(0) \in \Omega$ and $V(t)$ is piecewise continuous along the trajectory of the switched system consisting of $\mathcal{G}_1$ and $\mathcal{G}_2$, if $V(t)$ does not remain inside Ω for all $t \geq 0$, there exists $\tau_u > 0$ such that

$$V(t) \leq V_\Omega, \qquad t \in [0, \tau_u] \tag{A1a}$$

$$V(\tau_u) = V_\Omega \tag{A1b}$$

Therefore, for the V_b in Eq. (47) subject to inequality (48), we have

$$V(t) \leq e^{-\lambda_0(t-\tau-T_p)+\mu T_p} V(\tau) \leq e^{-\lambda_0(t-\tau)+(\lambda_0+\mu)[T_0+\alpha(t-\tau)]} V(\tau)$$
$$= e^{(\lambda_0+\mu)T_0-[\lambda_0-\alpha(\lambda_0+\mu)](t-\tau)} V(\tau) = e^{(\lambda_0+\mu)T_0-\lambda(t-\tau)} V(\tau) \tag{A2}$$

where

$$\lambda = \lambda_0 - \alpha(\lambda_0 + \mu) \tag{A3}$$

It is clear that the assumption (46a) ensures that $\lambda > 0$. Next, it is shown that $V(t)$ is upper bounded by $e^{(\lambda_0+\mu)T_0} V_b$ over $[0, \tau_u]$.

From Eq. (A2), for any $V(\tau) \geq V_b$, $V(t) \leq e^{(\lambda_0+\mu)T_0-\lambda(t-\tau)} V(\tau)$, for $\tau \leq t \leq \tau_u$. Suppose that, at time instant $t_1 \in [\tau, \tau_u]$, $V(t_1) \leq e^{(\lambda_0+\mu)T_0-\lambda(t_1-\tau)} V(\tau) \leq e^{(\lambda_0+\mu)T_0} V_b$. Then, for any $\tau \leq t_1 \leq t_2 \leq \tau_u$,

$$V(t_2) \leq e^{(\lambda_0+\mu)T_0-\lambda(t_2-\tau)} V(\tau) = e^{(\lambda_0+\mu)T_0-\lambda(t_1-\tau)} V(\tau) e^{-\lambda(t_2-t_1)}$$
$$\leq e^{(\lambda_0+\mu)T_0} V_b e^{-\lambda(t_2-t_1)} \leq e^{(\lambda_0+\mu)T_0} V_b \tag{A4}$$

Hence, if $V(\tau) \geq V_b$ for any $\tau \in [0, \tau_u]$, then $V(t)$ is ultimately upper bounded by $e^{(\lambda_0+\mu)T_0} V_b$ for $t \in [\tau, \tau_u]$. In summary, $V(t) \leq e^{(\lambda_0+\mu)T_0} V_b$, for $t \in [0, \tau_u]$. Because the relationships in inequalities (46b) and (48) ensure that $e^{(\lambda_0+\mu)T_0} V_b < V_\Omega$, then

$$V(t) \leq e^{(\lambda_0+\mu)T_0}V_b < V_\Omega, \quad \forall\ t \in [0, \tau_u] \tag{A5}$$

which contradicts Eq. (A1b). Therefore, the trajectory of the switched system remains inside Ω. Therefore, $V(t) \in \Omega$, $\forall\ t \geq 0$. Hence, inequalities (A2–A5) hold for all $t \geq 0$ and the switched system is uniformly ultimately bounded by $e^{(\lambda_0+\mu)T_0}V_b$ over Ω. This completes the proof. □

Acknowledgments

The authors would like to thank Chengyu Cao and Florent Lamiraux for their suggestions. Research is supported by the U.S. Army Special Operations Command, Office of Naval Research under contract N00014-05-1-0828, the U.S. Air Force Office of Scientific Research under contract FA9550-05-1-0157, and the U.S. Army Research Office under contract W911NF-06-1-0330.

References

[1] Gerten, G., "Protecting the Global Positioning System," *IEEE Aerospace and Electronic Systems Magazine*, Vol. 20, No. 11, 2005, pp. 3–8. doi:10.1109/MAES.2005.1576067

[2] Sridhar, B., and Suorsa, R., "Vision-Based Obstacle Detection for Rotorcraft Flight," *Journal of Robotic Systems*, Vol. 9, No. 6, 1992, pp. 709–727. doi:10.1002/rob.4620090603

[3] Suorsa, R., and Sridhar, B., "A Parallel Implementation of a Multisensor Feature-Based Range-Estimation Method," *IEEE Transactions on Robotics and Automation*, Vol. 10, No. 6, 1994, pp. 755–768. doi:10.1109/70.338530

[4] Petillot, Y., Ruiz, I., and Lane, D., "Underwater Vehicle Obstacle Avoidance and Path Planning Using a Multi-Beam Forward Looking Sonar," *IEEE Journal of Oceanic Engineering*, Vol. 26, No. 2, 2001, pp. 240–251. doi:10.1109/48.922790

[5] Costa, P., "Adaptive Model Architecture and Extended Kalman–Bucy Filters," *IEEE Transactions on Aerospace and Electronic Systems*, Vol. 30, No. 2, 1994, pp. 525–533. doi:10.1109/7.272275

[6] Farina, D., and Ristic, B., "Tracking a Ballistic Target: Comparison of Several Nonlinear Filters," *IEEE Transactions on Aerospace and Electronic Systems*, Vol. 38, No. 3, 2002, pp. 854–867. doi:10.1109/TAES.2002.1039404

[7] Christophersen, H., Pickell, R., Neidhoefer, J., Koller, A., Kannan, S., and Johnson, E., "A Compact Guidance, Navigation, and Control System for Unmanned Aerial Vehicles," *Journal of Aerospace Computing, Information, and Communication*, Vol. 3, No. 5, 2006, pp. 187–213. doi:10.2514/1.18998

[8] Langelaan, J., and Rock, S., "Navigation of Small UAVs Operating in Forests," AIAA Paper 2004-5140, 2004.

[9] Langelaan, J., "State Estimation for Autonomous Flight in Cluttered Environments," *Journal of Guidance, Control, and Dynamics*, Vol. 30, No. 5, 2007, pp. 1414–1426. doi:10.2514/1.27770

[10] Zarchan, P., and Alpert, J., "Using Filter Banks to Improve Interceptor Performance Against Weaving Targets," AIAA Paper 2006-6700, 2006.

[11] Oh, S., and Johnson, E., "Relative Motion Estimation for Vision-Based Formation Flight Using Unscented Kalman Filter," AIAA Paper 2007-6866, 2007.

[12] Soetanto, D., Lapierre, L., and Pascoal, A., "Adaptive Non-Singular Path Following Control of Dynamic Wheeled Robots," *International Conference on Informatics in Control, Automation, and Robotics*, Inst. of Electrical and Electronics Engineers, Los Alamitos, CA, 2003, pp. 1765–1770.

[13] Ghabcheloo, R., Pascoal, A., Silvestre, C., and Kaminer, I., "Non-Linear Co-Ordinated Path Following Control of Multiple Wheeled Robots with Bidirectional Communication Constraints," *International Journal of Adaptive Control and Signal Processing*, Vol. 21, No. 2–3, 2007, pp. 133–157. doi:10.1002/acs.923

[14] Ghabcheloo, R., Pascoal, A., Silvestre, C., and Kaminer, I., "Coordinated Path Following Control of Multiple Wheeled Robots Using Linearization Techniques," *International Journal of Systems Science*, Vol. 37, No. 6, 2006, pp. 399–414. doi:10.1080/00207720500438324

[15] Lamiraux, F., Bonnafous, D., and Lefebvre, O., "Reactive Path Deformation for Nonholonomic Mobile Robots," *IEEE Transactions on Robotics and Automation*, Vol. 20, No. 6, 2004, pp. 967–977. doi:10.1109/TRO.2004.829459

[16] Lefebvre, O., Lamiraux, F., and Bonnafous, D., "Fast Computation of Robot-Obstacle Interactions in Nonholonomic Trajectory Deformation," *IEEE International Conference on Robotics and Automation*, Inst. of Electrical and Electronics Engineers, New York, 2005, pp. 4612–4617.

[17] Boyer, F., and Lamiraux, F., "Trajectory Deformation Applied to Kinodynamic Motion Planning for a Realistic Car Model," *IEEE International Conference on Robotics and Automation*, Inst. of Electrical and Electronics Engineers, New York, May 2006, pp. 487–492.

[18] Hillion, M., and Lamiraux, F., "Taking Into Account Velocity and Acceleration Bounds in Nonholonomic Trajectory Deformation," *IEEE International Conference on Robotics and Automation*, Inst. of Electrical and Electronics Engineers, New York, April 2007, pp. 3080–3085.

[19] Quinlan, S., and Khatib, O., "Elastic Bands: Connecting Path Planning and Control," *IEEE International Conference on Robotics and Automation*, Inst. of Electrical and Electronics Engineers, New York, May 1993, pp. 802–807.

[20] Bowling, A., and Khatib, O., "Design of Non-Redundant Manipulators for Optimal Dynamic Performance," *IEEE International Conference on Advanced Robots*, Inst. of Electrical and Electronics Engineers, New York, July 1997, pp. 865–872.

[21] Hu, T., Kahng, A., and Robins, G.,"Optimal Robust Path Planning in General Environments," *IEEE Transactions on Robotics and Automation*, Vol. 9, No. 6, Dec. 1993, pp. 775–784. doi:10.1109/70.265921

[22] Ma, L., Cao, C., Hovakimyan, N., Woolsey, C., and Dixon, W., "Fast Estimation for Range Identification in the Presence of Unknown Motion Parameters," *IMA Journal of Applied Mathematics* (submitted for publication).

[23] Dippold, A., Ma, L., and Hovakimyan, N., "Vision-Based Obstacle Avoidance of Wheeled Robots Using Fast Estimation," AIAA Paper 2008-7449, 2008.

[24] Laumond, J., *Robot Motion Planning and Control*, Lecture Notes in Control and Information Sciences, Springer, New York, 1998.

[25] Reynolds, C., "Flocks, Herds and Schools: A Distributed Behavioral Model," *Computer Graphics*, Vol. 21, No. 4, 1987, pp. 25–34. doi:10.1145/37402.37406

[26] Hespanha, J., Yakimenko, O., Kaminer, I., and Pascoal, A., "Linear Parametrically Varying Systems with Brief Instabilities: An Application to Integrated Vision/IMU Navigation," *IEEE Transactions on Aerospace and Electronic Systems*, Vol. 40, No. 3, July 2004, pp. 889–902. doi:10.1109/TAES.2004.1337462

[27] Dobrokhodov, V., Kaminer, I., Jones, K., Kitsios, I., Cao, C., Ma, L., Hovakimyan, N., and Woolsey, C., "Rapid Motion Estimation of a Target Moving with Time-Varying Velocity," AIAA Paper 2007-6746, Aug. 2007.

[28] Ma, L., Cao, C., Hovakimyan, N., Dobrokhodov, V., and Kaminer, I., "Adaptive Vision-Based Guidance Law with Guaranteed Performance Bounds for Tracking a Ground Target with Time-Varying Velocity," AIAA Paper 2008-7445, Aug. 2008.

[29] Dobrokhodov, V., Kaminer, I., Jones, K., and Ghabcheloo, R., "Vision-Based Tracking and Motion Estimation for Moving Targets Using Unmanned Air Vehicles," *Journal of Guidance, Control, and Dynamics*, Vol. 31, No. 4, July–Aug. 2008, pp. 907–917. doi:10.2514/1.33206

[30] Khalil, H., *Nonlinear Systems*, Prentice–Hall, Englewood Cliffs, NJ, 2002.

[31] Dippold, A., "Vision-Based Obstacle Avoidance for Multiple Vehicles Performing Time-Critical Missions," Ph.D. Thesis, Virginia Polytechnic Institute and State University, Blacksburg, VA, 2009.